PERGAMON

International Journal of Heat and Mass Transfer 45 (2002) 3189–3197

International Journal of HEAT and MASS TRANSFER

www.elsevier.com/locate/ijhmt

Unified theoretical prediction of fully developed nucleate boiling and critical heat flux based on a dynamic microlayer model

Yao-Hua Zhao [a,*], Takashi Masuoka [b], Takaharu Tsuruta [c]

[a] *Institute of Engineering Thermophysics, Chinese Academy of Sciences, Beijing 100080, China*
[b] *Department of Mechanical Engineering and Science, Kyushu University, Fukuoka 812-8581, Japan*
[c] *Department of Mechanical Engineering, Kyushu Institute of Technology, Kitakyushu 804-8550, Japan*

Received 24 October 2001

Abstract

A new dynamic microlayer model has been proposed to predict theoretically the heat flux in fully developed nucleate boiling regions including critical heat flux (CHF). In this model, the heat transfer with boiling is mainly attributed to the evaporation of the microlayers which are periodically formed while the individual bubbles are forming. Since the initial microlayer thickness becomes thinner with the increase of wall superheat, both the local evaporation and the partial dryout speed of the microlayer increase. As a result, the time-averaged heat flux during the period of individual bubble has a maximum point, the CHF, at the predicted continuous boiling curve. © 2002 Elsevier Science Ltd. All rights reserved.

1. Introduction

A significant amount of research on the critical heat flux (CHF) of boiling heat transfer has been published because of its practical and academic importance in thermal engineering. Comprehensive reviews have been presented by Katto [1] and Lienhard [2].

The main analytical models on CHF in previous studies may be divided into two categories: the hydrodynamic instability model and the macrolayer dryout model.

The hydrodynamic instability model, also termed as "far-field model", was first presented in the foundation work of Zuber [3] for predicting the CHF in saturated pool boiling over horizontal surfaces. It was further developed to evaluate the CHF for pool boiling on wires, ribbons, etc. by Lienhard et al. [4]. This model has been extensively used because its final correlation takes the same form as the semi-empirical one by Kutatelatze [5].

The macrolayer dryout model, also termed as "near-surface model", was proposed by Haramura and Katto [6] based on a series of experimental observations including Gaertner's [7], which seem much different from the physical model used by Zuber [3] for pool boiling on horizontal surfaces. This model postulates that a liquid sublayer (macrolayer) formed on the heater surface with an initial thickness is evaporated away during a hovering period of the overlying vapor mass when the CHF appears. The macrolayer dryout model is based on the condition of the dryout of the macrolayer without liquid resupply throughout the period of vapor mushroom.

Ideas have been proposed to explain the complex phenomena of CHF in both of the above models which disregard the detailed processes of heat and mass transfer on the boiling surfaces, so that, the fluid and solid contact structures have been greatly simplified and assumed to be time-independent.

The on-wall mechanism had not been considered either of the two above models, some attempts have been

* Corresponding author. Tel./fax: +86-10-8287-1076.
E-mail address: yhzhao@mail.etp.ac.cn (Y.-H. Zhao).

PII: S0017-9310(02)00022-4

Nomenclature

A_b	microlayer area $(=\pi(d/2)^2)$
A_d	the largest cross-sectional area of individual bubble
c_p	specific heat of liquid
D_d	departure diameter of individual bubble
D_t	instantaneous diameter of individual bubble
d	diameter of individual bubble at the end of initial growth
g	gravitational constant
h_{fg}	latent heat of evaporation
k_l	thermal conductivity
N	number of active sites in unit area
q	wall heat flux
q_c	transient heat conduction in the liquid macrolayer
q_{ev}	evaporation heat flux on microlayer
R	radius of individual bubble
r	coordination
r_c	position at which the superheat boundary layer reaches the liquid–vapor interface
$r^d_{(t)}$	radius of dryout area
s	normal distance of center of gravity of individual bubble above heated surface
t	time
t_g	period of initial growth
T	temperature
ΔT_{sat}	wall superheat
V	volume of bubble
v_l	volumetric growth rate of bubble
t_d	departure time period

Greek symbols

α	thermal diffusivity of liquid
θ	contact angle
δ	thickness
δ^0	initial thickness
λ_C	Taylor instability wavelength
λ_D	most dangerous Taylor instability wavelength
ρ	density
σ	surface tension
ξ	volumetric ratio of accompanying liquid to the moving bubble

Subscripts

d	individual bubble
D	vapor mushroom
g	initial growth
l	liquid
ma	macrolayer
mi	microlayer
v	vapor

made to explain the detailed processes of heat and mass transfer on the boiling surfaces. A group of studies have been performed by Nelson and his co-workers [8] based on the macrolayer dryout model, in which the dominant heat transfer is attributed to the evaporation at the liquid–vapor–solid contact points (so called triple points). Another group of studies have been performed by Dhir and Liaw [9,10], in which the heat flux is related to the void fraction. By employing experimentally observed void fraction, the nucleate boiling (at high heat flux region) and transition boiling heat fluxes including the maximum and minimum heat fluxes are predicted from the model. Furthermore, Lay and Dhir [11] have proposed a vapor stem model and made a dynamic analysis of it, from which stable vapor stem is possible. Those models have shown that only the evaporation of a so-called microlayer (which is much thinner than the macrolayer) can contribute the high heat flux in fully developed nucleate boiling. These two kinds of models seem to be successful to predict CHF in a variety of situations. However, many questions about both of the two models have been raised. A detailed review of those questions has recently been made by Sadasivan et al. [13]. We classified certain problems of popular concern and made a conceptual approach to new model as follows:

1.1. Hydrodynamic instabilities

The far-field, hydrodynamic instabilities usually refer to two types: the Taylor instability along with boiling surfaces, and the Kelvin–Helmholtz instability along with the vapor escape path. The Taylor instability is very likely to occur once the vapor width is larger than the instability wave length, so as to play a dominant role in the width of departure vapor-mushroom. However, for many boiling surfaces, even for enhanced heat transfer surfaces such as some porous surfaces on which the CHF can be up to about twice of that in usual pool boiling, the hydrodynamic instability model can give a unique value of CHF. This implies that some other mechanisms should have to work on CHF at least for usual pool boiling. The CHF for pool boiling with very low-level liquid clarifies also that, the Kelvin–Helmholtz instability does not work if CHF reached a usual value. So, it seems to follow that, a hydrodynamic instability model would give an upper limit of CHF much higher

than that predicted by Zuber [3], if the hydrodynamic instability really dominates the CHF.

1.2. Liquid resupply

Two kinds of liquid resupply processes have been discussed in previous studies: the intermittent resupply ofliquid to the macrolayer with the period of vapor mushroom, and the continuous replenishment of the macrolayer. The former is clarified by investigators such as Yu and Mesler [12]; the latter seems to be impossible as concluded by Sadasivan et al. [13]. However, we consider that the continuous replenishment of the macrolayer does exist based on the experimental evidence [14–16].

Sakashita et al. [14] developed a method to measure the thickness of macrolayers and clarified that the thickness of macrolayer in a free pool boiling is thicker than that in a confined space boiling in which no liquid is resupplied. Furthermore, as is popularly known, the boiling time can be maintained over several seconds near the CHF at 1g [15,16]. By using the macrolayer dryout model, the thickness of the macrolayer could be about several millimeters as being visible, but the practical measured macrolayer thickness is in order of 100 μm, and the macrolayer would dry out quickly if no liquid is resupplied. So, continuous liquid supply may result that the CHF does not depend on the initial thickness of the macrolayer and the period of vapor mushroom.

1.3. Effect of gravity

The CHF under microgravity is independent or only weakly dependent on the level of gravity especially for water boiling [15,16]. This seems to be in contradiction with the prediction based on the hydrodynamic instability model and the macrolayer dryout model. The role of the gravity on CHF must be questionable thereby. It seems from the CHFs both with very low-level liquid mentioned above, and at microgravity that some other mechanism on CHF exists, which is independent or only a weak function of gravity.

1.4. Microlayer and macrolayer

It has been clarified that only the evaporation on the microlayer (which is much thinner than the macrolayer) can contribute the high heat flux at CHF, i.e. the microlayer would be useful to explore the mechanism of the detailed evaporation process. Up to now, two kinds of microlayers have been studied: the thin liquid layer formed while a bubble is forming, the microlayer in the vicinity of the stationary meniscus interline which has an extremely small area. The typical studies on the thin liquid layer were performed by Cooper et al. [17,18], such a microlayer is the same as the bottom area of the bubbles on the wall. This microlayer has an extremely small area. According to our knowledge, no studies have shown that the evaporation at the second kind of microlayer can match the actual mean wall heat flux near the CHF at the usual pool boiling even if a uniform wall temperature is assumed. If the conjugated heat transfer between the heater wall and the boiling liquid is considered, it seems to be more difficult to explain the mechanism of high heat flux by the second kind of stationary microlayer. In the following sections, the microlayer referred is of the first kind.

Regarding the macrolayer, at least for the pool boiling of R113 on a horizontal plate, the experimental observations by Nishio et al. [20] show that the macrolayers never dry away not only at CHF point but also in transition boiling. In their study, the isolated dry-points and their developing processes without the dryout of the macrolayer are observed near the CHF point.

1.5. Individual bubbles within macrolayer

Experimental observations on water boiling [19] and R113 boiling [20] show clearly that the individual boiling bubbles are formed and depart periodically from the boiling surfaces. The vapor stems and the dryout of macrolayer have not been observed near CHF. The dynamic distribution of liquid layer near the wall measured, including the recent report of Hohl et al. [21], supports the periodical existence of the individual bubbles instead of the stationary vapor stems.

1.6. Fluctuation of local wall temperature

The fluctuation of local wall temperature was detected even for the transition boiling [22,23]. The periods of the spatial temperature variations on the boiling surface are about several milliseconds which are one order less than the periods of vapor mushroom. It implies that the practical micro-structure of liquid layer on the wall should be time-dependent during the period of developing a vapor mushroom. One reasonable explanation for the fluctuations of local wall temperature may result from conjugated heat transfer between the heater surface and the fluid side corresponding to the periodic growth and departure of the individual bubbles within the macrolayer.

In short, a successful CHF model should be at least:

(a) time- and position-dependent to explain the local wall temperature fluctuation;
(b) based on a microlayer structure to match the high heat flux;
(c) continuous boiling curve near CHF to consider the effects of wall superheat;
(d) weakly dependent on the gravity to match the experimental results;

(e) possible to be developed to consider the effects of the surface parameters.

The objective of the present work is to theoretically investigate the CHF mechanism based on an on-surface model, a microlayer model, by focusing on the behaviors of individual bubbles beneath the vapor mushroom. The developing process of the isolated dry-areas beneath individual bubbles results in the critical heat flux, i.e. the wall heat flux reaching its critical value (CHF) with the increasing wall superheat.

2. Microlayer model proposed for fully developed nucleate boiling and CHF

2.1. Basic idea

As shown in Fig. 1, the growth of individual bubbles can be divided into two periods, i.e. the initial growth period and the final growth period. During the initial growth period, the bubbles grow in a semi-spherical shape with microlayer formed beneath it. The shape of bubble changes from the semi-spherical to the spherical segment geometry due to the evaporation of the microlayer. In the final growth period, a liquid layer thicker than the microlayer is formed under the bubble and among the adjacent individual bubbles. This layer is termed macrolayer in this paper.

The formation mechanism of the microlayer has been studied both theoretically and experimentally by Cooper et al. [18] and its thickness can be expressed by the following equation:

$$\delta_{\mathrm{mi}}^{0} = 0.8\sqrt{\nu_{\mathrm{l}} t} = \sqrt{c\alpha \cdot t}, \quad 0 \leqslant t \leqslant t_{\mathrm{g}}, \tag{1}$$

where $c = 0.64Pr$. Here the effect of surface tension can be neglected because the duration of initial growth is usually very short.

In the nucleate boiling under high heat flux condition, the individual bubbles under the coalescence bubble (or vapor mushroom) are generated and depart from the heated surface periodically. Fig. 2 shows the physical model for explaining the configuration of individual bubbles, the vapor mushroom and micro/macro-layers. Two situations are depicted depending on the departing mechanism of the individual bubbles. For fluids with a large value of $k_{\mathrm{l}}\rho_{\mathrm{l}}c_{\mathrm{pl}}$ such as water, the growth rate is fast and the interface between the individual bubbles and vapor mushroom can be easily broken down. As a result, the coalescence occurs in the normal direction. For small $k_{\mathrm{l}}\rho_{\mathrm{l}}c_{\mathrm{pl}}$ fluids like fluorocarbons, the growth rate is slow and the coalescences occur among the individual bubbles on the surface. The center distance between the individual bubbles is $2d$ in the case (a) and D_{d} in the case (b), respectively. In both cases, the micro and macrolayers exist on the heated surface under the individual bubbles and the macrolayer is never dried out due to a continuous liquid resupply.

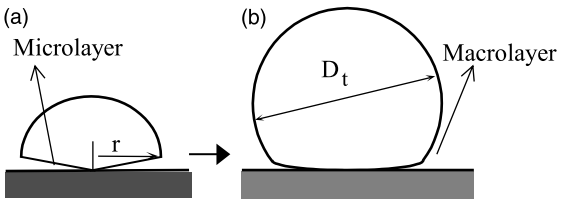

Fig. 1. Dynamic micro/macrolayers: (a) initial growing stage; (b) final growing stage.

The heated surface can be divided into three regions: the dryout area, the microlayer area and the macrolayer area. The evaporation occurs mainly at the microlayer area, whereas the evaporation of the liquid macrolayer is small and can be neglected. The areas of the three parts change with time. The dryout region with a zero initial area develops due to the evaporation of the liquid microlayer during the period of the individual bubble. As a result, the microlayer area decreases with time. Here, it is supposed that no liquid is resupplied into the tremendously thin microlayer, because of the very small interfacial curvature. After individual bubbles depart from the boiling surface, the old microlayer area is replaced by fresh liquid from the macrolayer.

We assume that the surface temperature being uniform throughout the boiling surface and keeping a constant value during the period of vapor mushroom, and neglect the waiting time of nucleation. Then, the local surface flux can be given as follows:

$$q_{(r,t)} = \begin{cases} 0, & r \leqslant r_{(t)}^{\mathrm{d}}, \\ -\rho_{\mathrm{l}} h_{\mathrm{fg}} \frac{\mathrm{d}\delta_{\mathrm{mi}}}{\mathrm{d}t}, & r_{(t)}^{\mathrm{d}} < r \leqslant d/2, \\ -\rho_{\mathrm{l}} h_{\mathrm{fg}} \frac{\mathrm{d}\delta_{\mathrm{ma}}}{\mathrm{d}t}, & d/2 < r \leqslant r_{\mathrm{c}}, \\ q_{\mathrm{c}}, & r \geqslant r_{\mathrm{c}}, \end{cases} \tag{2}$$

where $r_{(t)}^{\mathrm{d}}$ is the radius of dryout area. δ_{mi} and δ_{ma} are the microlayer and macrolayer thicknesses, respectively. The heat flux in the dryout area is small enough to be neglected. The heat flux q_{c} in the macrolayer area can be evaluated by the periodically transient heat conduction in a semi-infinite liquid layer with the bulk temperature of $(T_{\mathrm{w}} + T_{\mathrm{sat}})/2$.

The mean wall heat flux can be derived accordingly from Eq. (2):

$$\begin{aligned} \bar{q}_{\mathrm{w}} = \frac{1}{A_{\mathrm{d}} t_{\mathrm{d}}} \Bigg[& \int_0^{t_{\mathrm{d}}} \int_{A_{\mathrm{b}}} \left(-\rho_{\mathrm{l}} h_{\mathrm{fg}} \frac{\mathrm{d}\delta_{\mathrm{mi}}}{\mathrm{d}t} \right) \mathrm{d}A\, \mathrm{d}t \\ & + \int_0^{t_{\mathrm{d}}} \int_{\pi r_{\mathrm{c}}^2 - A_{\mathrm{b}}} \left(-\rho_{\mathrm{l}} h_{\mathrm{fg}} \frac{\mathrm{d}\delta_{\mathrm{ma}}}{\mathrm{d}t} \right) \mathrm{d}A\, \mathrm{d}t \\ & + \int_0^{t_{\mathrm{d}}} \int_{A_{\mathrm{d}} - A_{\mathrm{b}}} q_{\mathrm{c}}\, \mathrm{d}A\, \mathrm{d}t \Bigg], \end{aligned} \tag{3}$$

where t_{d} is the departure period of the individual bubble.

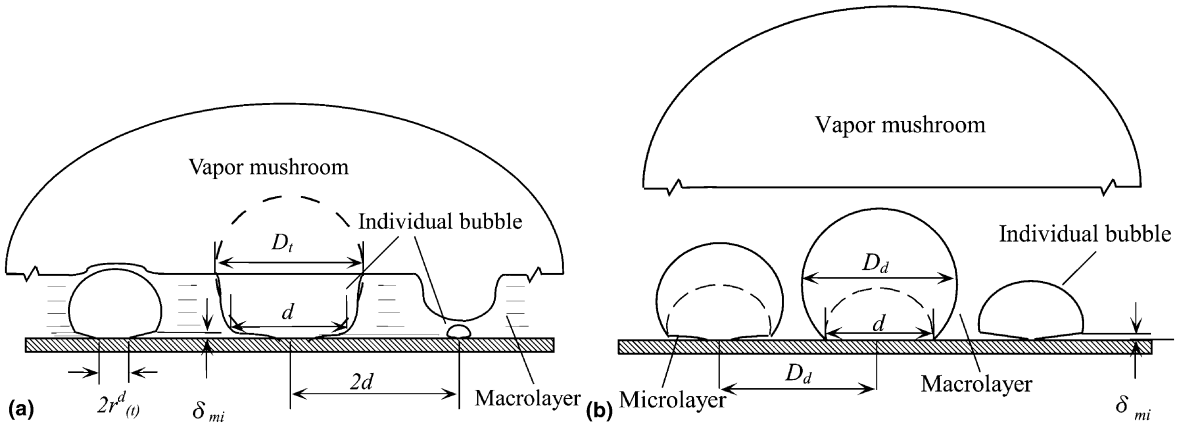

Fig. 2. Physical model: (a) coalescence into vapor mushroom; (b) coalescence among individual bubbles.

Eq. (2) indicates that the instantaneous heat flux in microlayer region increases with decreasing microlayer thickness. As to be shown in Section 2.2, the initial thickness of the microlayer decreases with increasing wall superheat. A thinner microlayer causes faster development of dryout area. These two aspects result in the fact that the heat flux has a maximum value which is just the CHF, and satisfy the corresponding condition:

$$\partial \bar{q}_w/\partial \Delta T_{sat} = 0 \quad \text{as } \Delta T_{sat} = \Delta T_{sat}^{CHF}. \tag{4}$$

2.2. The initial growth of individual bubbles

As shown in Fig. 1, the growth of the individual bubble is characterized by two different growing mechanisms. In the initial growing stage, the effect of heat transfer is dominant, while the kinetic effect plays an important role in the final growing stage. The whole period t_d for the bubble growth should be divided into two stages: the initial growth stage for $0 \leqslant t \leqslant t_g$, and the final growth stage for $t_g < t \leqslant t_d$, t_d being the departure time.

During the initial growth of the individual bubbles, the semi-spherical bubbles grow from active nuclei. The growth equation of individual bubbles can be derived from the heat balance between the latent heat of evaporation of the liquid microlayer and the conduction heat through the microlayer. That is,

$$\frac{2}{3}\pi R^3 \rho_v h_{fg} = 2\pi k_l \int_0^R \int_{t_g}^t \frac{\Delta T_s}{\delta_{mi}} r \, dt \, dr, \quad 0 \leqslant t \leqslant t_g, \tag{5}$$

where t_g is the time while the liquid microlayer is just formed.

In nucleate boiling region, when the wall superheat is not high, the following approximation can be made:

$$\frac{2}{3}\pi R^3 \rho_v h_{fg} \approx 2\pi k_l \int_0^R \int_0^t \frac{\Delta T_s}{\delta_{mi}} r \, dt \, dr, \quad 0 \leqslant t \leqslant t_g. \tag{6}$$

By utilizing Cooper's equation (1), the bubble radius is obtained as

$$R \equiv r = \frac{2k_l \Delta T_{sat}}{\rho_v h_{fg} \sqrt{c\alpha}} t^{1/2}. \tag{7}$$

At the end of the initial growth of individual bubble, i.e. at $t = t_g$, the bubble diameter d will be

$$d = \frac{4k_l \Delta T_{sat}}{\rho_v h_{fg} \sqrt{c\alpha}} t_g^{1/2}. \tag{8}$$

From Eq. (6), we can obtain the time t_g at which the front edge of the semi-spherical bubble with the radius R reaches the radial position r, where the bubble radius is the same as the coordinate position, i.e.

$$t_g = \left[\frac{\sqrt{c\alpha}\rho_v h_{fg} r}{2k_l \Delta T_{sat}}\right]^2, \quad r \leqslant d/2. \tag{9}$$

So the initial thickness of microlayer at any position r ($r \leqslant d/2$) can be given as

$$\delta_{mi}^0 = \sqrt{c\alpha \cdot t_g} = \frac{c\alpha \rho_v h_{fg} r}{2k_l \Delta T_{sat}}. \tag{10}$$

2.3. Bubble dynamics

During the final growth period, the growth of individual bubbles is governed by the bubble dynamics. The forces acting on the bubbles are illustrated in Fig. 3.

Equation of motion is given as follows by considering the forces due to inertia, buoyancy and surface tension:

$$\begin{cases} \frac{d}{dr}\left[(\xi\rho_l + \rho_v) V \frac{ds}{dt}\right] = (\rho_l - \rho_v) Vg + f(\sigma), & t > t_g, \\ s = \frac{3k_l \Delta T_{sat}}{4\rho_v h_{fg}\sqrt{c\alpha}} t^{1/2}, & t \leqslant t_g, \end{cases} \tag{11}$$

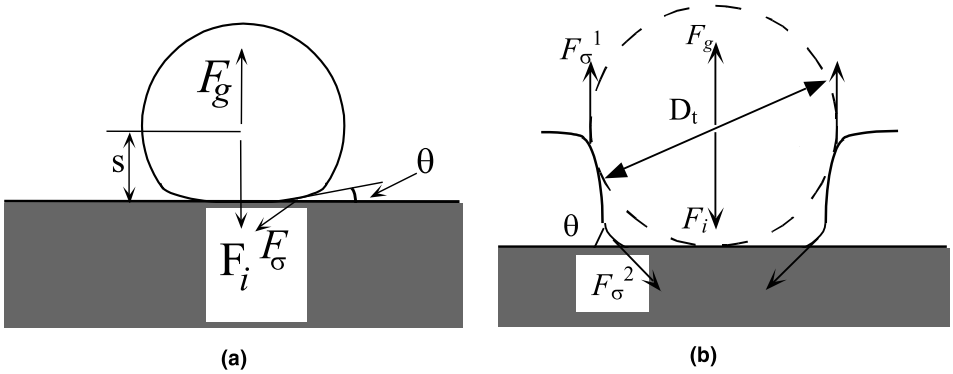

Fig. 3. Forces acting on departing bubble: (a) isolated bubble; (b) bubble coalescing into vapor mushroom.

where for the case of non-absorption, $\xi = 11/16$, which is the volumetric ratio of the accompanying liquid to the moving bubble [6], $f(\sigma) = 2\pi r_{(t)}^{\mathrm{d}}\sigma\sin\theta$; for the case of coalescence between the individual bubble and the vapor mushroom, $\xi = 11/32$, $f(\sigma) = \pi\sigma[d - 2r_{(t)}^{\mathrm{d}}\sin\theta]$. s is the vertical distance between the weight center of bubble and the wall. V is the volume of bubble obtained by the following equation:

$$V = \frac{1}{12}\pi d^3 + \int_{t_{\mathrm{g}}}^{t} v_1\,\mathrm{d}t, \quad v_1 = \frac{\pi d^2 q_{\mathrm{ev}}}{\rho_{\mathrm{v}} h_{\mathrm{fg}}}, \tag{12}$$

where v_1 is the volume growth rate.

The relationship at the departure time of individual bubble ($t = t_{\mathrm{d}}$) can be derived as

$$\begin{aligned}(\xi\rho_{\mathrm{l}} + \rho_{\mathrm{v}})\left(\frac{1}{12}\pi d^3 + \int_{t_{\mathrm{g}}}^{t} v_1\,\mathrm{d}t\right)\left.\frac{\mathrm{d}s}{\mathrm{d}t}\right|_{t=t_{\mathrm{d}}} &= (\xi\rho_{\mathrm{l}} + \rho_{\mathrm{v}})\frac{1}{12}\pi d^3\left.\frac{\mathrm{d}s}{\mathrm{d}t}\right|_{t=t_{\mathrm{g}}} + \frac{1}{12}\pi d^3(\rho_{\mathrm{l}} - \rho_{\mathrm{v}})g(t_{\mathrm{d}} - t_{\mathrm{g}}) \\ &\quad + (\rho_{\mathrm{l}} - \rho_{\mathrm{v}})g\int_{t_{\mathrm{g}}}^{t_{\mathrm{d}}}\int_{t_{\mathrm{g}}}^{t} v_1\,\mathrm{d}t\,\mathrm{d}t + \int_{t_{\mathrm{g}}}^{t_{\mathrm{d}}} f(\sigma)\mathrm{d}t.\end{aligned} \tag{13}$$

The first term on the right-hand side of Eq. (13) is the inertial one induced by the initial growth of the individual bubble. In the case that the individual bubble is merged into the vapor mushroom, the surface tension at the interface between them promotes the bubble departure from the heated surface.

The departure diameter D_{d} can be given by

$$D_{\mathrm{d}} = \left[\frac{1}{2} + \frac{6}{\pi d^3}\int_{t_{\mathrm{g}}}^{t_{\mathrm{d}}} v_1\,\mathrm{d}t\right]^{1/3}\cdot d. \tag{14}$$

2.4. Microlayer thickness and dryout area

The dryout area of the liquid microlayer can be obtained by considering the change of the thickness of the microlayer with time.

The consumption of the liquid microlayer due to evaporation is caused by the heat conducted from the heating surface through the microlayer:

$$-\rho_{\mathrm{l}} h_{\mathrm{fg}}\frac{\mathrm{d}\delta_{\mathrm{mi}}}{\mathrm{d}t} = \frac{k_{\mathrm{l}}\Delta T_{\mathrm{sat}}}{\delta_{\mathrm{mi}}}, \quad \delta_{\mathrm{mi}}^0 = \sqrt{c\alpha\cdot t_{\mathrm{g}}}. \tag{15}$$

Hence, the thickness of the microlayer can be derived as

$$\delta_{\mathrm{mi}} = \frac{c\alpha\rho_{\mathrm{v}} h_{\mathrm{fg}} r}{2k_{\mathrm{l}}\Delta T_{\mathrm{s}}}\cdot\left[1 - \frac{8c_{\mathrm{pl}}k_{\mathrm{l}}^2\Delta T_{\mathrm{sat}}^3(t - t_{\mathrm{g}})}{c^2\alpha h_{\mathrm{fg}}^3\rho_{\mathrm{v}}^2 r^2}\right]^{1/2}. \tag{16}$$

Therefore, the radius of dryout area ($\delta_{\mathrm{mi}} = 0$) will be

$$r_{(t)}^{\mathrm{d}} = \left[\frac{8c_{\mathrm{pl}}k_{\mathrm{l}}^2\Delta T_{\mathrm{sat}}^3(t - t_{\mathrm{g}})}{c^2\alpha h_{\mathrm{fg}}^3\rho_{\mathrm{v}}^2}\right]^{1/2}. \tag{17}$$

3. Prediction results and discussion

Substituting Eqs. (2) and (16) into Eq. (3) and neglecting the higher order terms of $(r_{(t)}^{\mathrm{d}})^2/d^2$, the mean wall heat flux can be derived as

$$\begin{aligned}\bar{q}_{\mathrm{w}} &= \frac{2k_{\mathrm{l}}^2 d\Delta T_{\mathrm{sat}}^2}{c\alpha\rho_{\mathrm{v}} h_{\mathrm{fg}} A_{\mathrm{d}}}\left[1 - \frac{8c_{\mathrm{pl}}k_{\mathrm{l}}^2\Delta T_{\mathrm{sat}}^3 t_{\mathrm{d}}}{c^2\alpha h_{\mathrm{fg}}^3\rho_{\mathrm{v}}^2 d^2}\right] \\ &\quad + \left(1 - \frac{\pi d^2}{4A_{\mathrm{d}}}\right)\frac{2k_{\mathrm{l}}\Delta T_{\mathrm{sat}}}{\sqrt{\pi\alpha t_{\mathrm{d}}}}.\end{aligned} \tag{18}$$

The CHF can thus be calculated out. If the diameter d (or D_{d}) is known.

For water, the calculated q_{CHF} is plotted as a function of d in Fig. 4 for contact angle $\theta = 22°$, and the regression relationship between them is obtained as

$$q_{\mathrm{CHF}} = 4.5\times 10^4 d^{-0.44}. \tag{19}$$

By using the experimental result by Gaertner [24], concerning the relationship between the density of active sites, N, and the heat flux, q,

$$q = 117.1N^{2/3}, \tag{20}$$

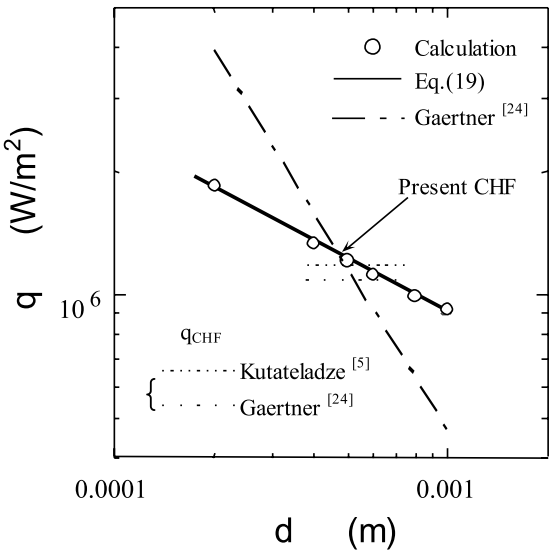

Fig. 4. CHF vs. d (water).

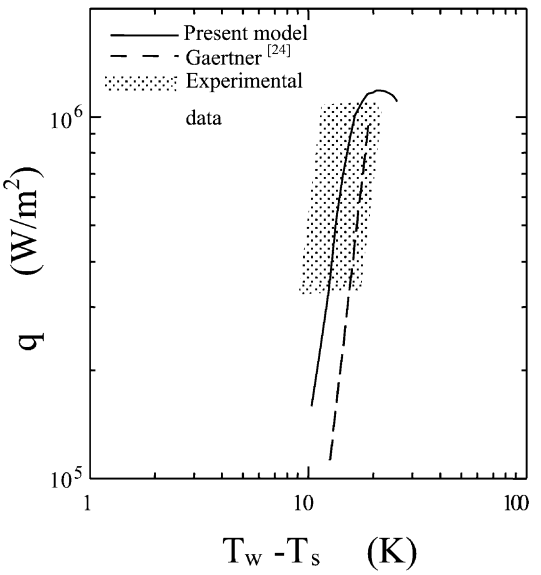

Fig. 5. Boiling curve of water.

the diameter of individual bubble can be given:

$$d = 17.8q^{-0.75}. \tag{21}$$

The following results can be obtained from Eqs. (18) and (21) for the CHF point for water under atmospheric pressure:

$$d = 0.5 \text{ mm}, \quad \Delta T_{\text{sat}} \approx 20.9 \text{ K},$$
$$q_{\text{CHF}} = 1.2 \times 10^6 \text{ W/m}^2.$$

In Fig. 4, the present result of q_{CHF} agrees well with the data reported [5,24].

With the present model for individual bubbles shown in Fig. 2, the predicted heat flux in fully developed nucleate boiling region is plotted in Fig. 5, good agreement between the present analytical results and experimented data reported in the literature is shown. The calculated mean dryout area fraction at the CHF is predicted at about 16.5%, which is very close to the result obtained by Shoji [25] for water.

The relation of q_{CHF} and D_{d} for R-12 is shown in Fig. 6. At CHF, the departure size of the individual bubble is about 1.2 mm and the bubble density is about $7 \times 10^5/\text{m}^2$.

The calculated departure periods of individual bubbles are plotted in Fig. 7. It is not a monotonic function of wall superheat, a peak value exists near the CHF. The predicted bubble departure periods and the fluctuation periods of local wall temperature are in same order with that measured by experiments [22,23]. Also, the detected dynamic signals of the liquid–vapor fluctuations near the boiling surface by Hohl et al. [21] can be easily explained by the present results.

Thus, it seems that the proposed microlayer model is successful to predict the heat transfer in fully developed nucleate boiling regions including the CHF, though as a first step, we have not considered the local temperature distribution which exists in practice because the local heat flux varies along with the r-position under the individual bubble. The effects of the material properties of the boiling surfaces can be clarified by the conjugated heat transfer between solid wall and fluid in future.

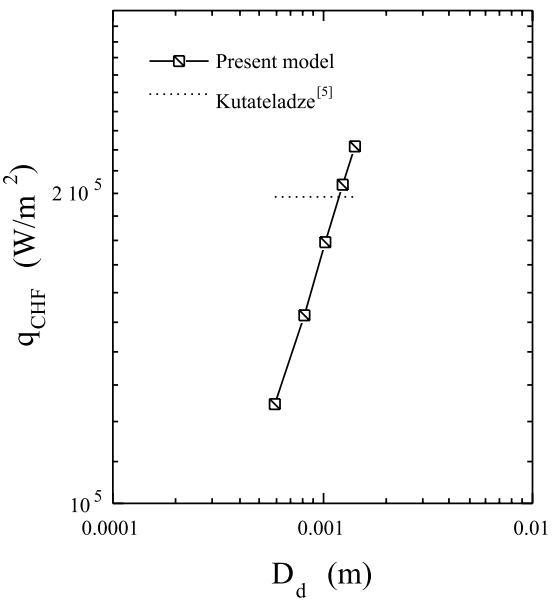

Fig. 6. Relationship between CHF and D_{d} for R-12.

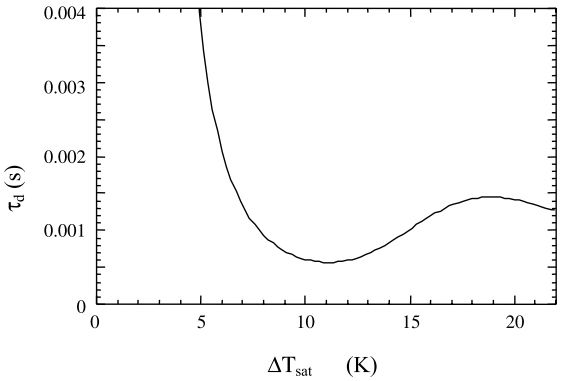

Fig. 7. t_d vs. T_{sat} for water.

Furthermore, the effect of the coalescences among the individual bubbles is disregarded in present microlayer model. For actual pool boiling, such coalescences should occur at some concentrated areas of the active sites. However, we think that, the coalescence will have no significant effect on the mean wall heat flux because such coalescences are occasional and the microlayer areas are little affected by the coalescence process for usual unconfined pool boiling.

It should be pointed out that the previous models have difficulty to explain the high value of CHF for the case of micro-gravity field and low-level boiling liquid (or thin liquid film), especially for water, because those predicted CHFs depend on the gravity (the departure of vapor mushroom is mainly driven by the gravity). The present model can explain those phenomena because the departure of individual bubbles is mainly driven by

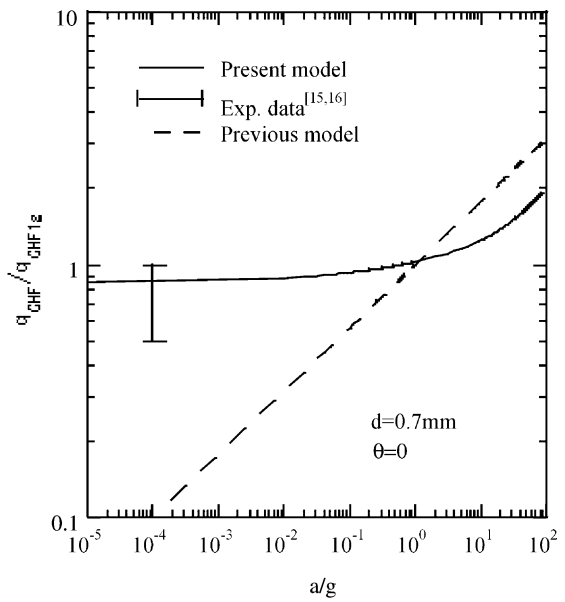

Fig. 8. Effect of gravity on CHF (water).

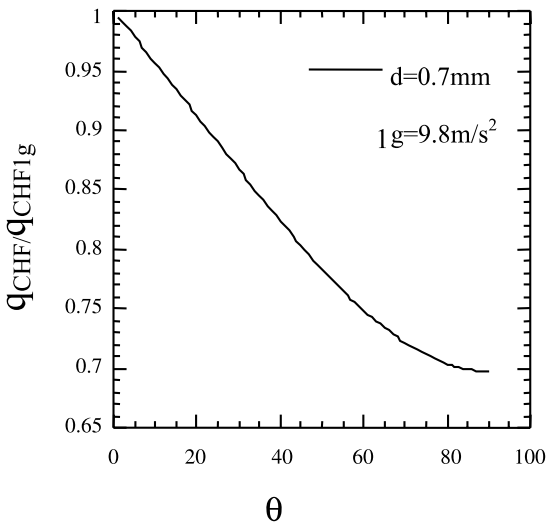

Fig. 9. Effect of contact angle on CHF.

the surface tension and the inertial force induced in the initial growth of the individual bubbles at the micro-gravity. Fig. 8 shows the effect of the gravity on the CHF. The CHF predicted by proposed model approaches a constant as the gravity level is reduced.

The predicted effect of contact angle on CHF is shown in Fig. 9 for water. The CHF decreases with increasing contact angle because a larger contact angle results in a longer departure period of individual bubble (Eq. (9)).

Furthermore, with the proposed microlayer model, the departure periods of the individual bubbles significantly affect the CHF which increases with decreasing departure period. It seems to be possible to develop the present model to predict the heat flux in forced convective boiling if the liquid inertia forces acting on the individual bubbles are considered. For possible engineering applications in practice, this model indicates that CHF will be augmented if the departure of the individual bubbles is promoted.

4. Conclusions

For pool boiling on horizontal surfaces, a new microlayer model is proposed to predict theoretically the heat transfer in fully developed nucleate boiling regions including CHF. The present model gives a dynamic structure of vaporliquid–solid contacts. The boiling heat transfer is mainly attributed to the evaporation of the microlayer which is formed during the initial growth period of individual bubbles. By considering the bubble dynamics, the microlayer thickness and the dryout area as well as the wall heat flux are formulated as the functions of superheat, a continuous boiling curve is

predicted. The initial thickness of the microlayer becomes thinner with increasing of wall superheat, both the evaporation and the partial dryout speed of the microlayer increase. As a result, the time-averaged heat flux during the departure period of individual bubble has a maximum point on the plane of q vs. ΔT_{sat}. This maximum heat flux for nucleate boiling is the CHF. The prediction of this model shows good agreement with experimental data available in the literature.

References

[1] Y. Katto, Critical heat flux, Int. J. Multiphase Flow 20 (Suppl.) (1994) 53–90.

[2] J.H. Lienhard, Snares of pool boiling research: putting our history to use, in: Proc. 10th Int. Heat Transfer Conf., Brighton, UK, vol. 1, 1994, pp. 333–348.

[3] N. Zuber, On the stability of boiling heat transfer, Trans. ASME J. Heat Transfer 80 (3) (1958) 711–720.

[4] J.H. Lienhard, V.K. Dhir, Hydrodynamic prediction of peak pool-boiling heat fluxes from finite bodies, Trans. ASME J. Heat Transfer 95 (1973) 152–158.

[5] S.S. Kutateladze, A hydromechanical heat transfer crisis model in a boiling liquid with free convection, Zh. Tekhc. Fiz. (ЖТф) 20 (11) (1950) 1389–1392.

[6] Y. Haramura, Y. Katto, A new hydrodynamic model of critical heat flux, applicable widely to both pool and forced convection boiling on submerged bodies in saturated liquids, Int. J. Heat Mass Transfer 26 (1983) 389–399.

[7] R.F. Gaertner, Photographic study of nucleate pool boiling on a horizontal surface, Trans. ASME J. Heat Transfer 87 (1965) 17–29.

[8] K.O. Pasamehmetoglu, P.R. Chappidi, C. Unal, R.A. Nelson, Saturated pool nucleate boiling mechanisms at high heat fluxes, Int. J. Heat Mass Trans. 36 (1993) 3859–3868.

[9] S.P. Liaw, V.K. Dhir, Void fraction measurements during saturated pool boiling of water on partially wetted vertical surfaces, Trans. ASME J. Heat Transfer 111 (1989) 731–738.

[10] V.K. Dhir, S.P. Liaw, Framework for a unified model for nucleate and transition pool boiling, Trans. ASME J. Heat Transfer 111 (1989) 739–746.

[11] J.H. Lay, V.K. Dhir, Shape of a vapor stem during nucleate boiling of saturated liquids, Trans. ASME J. Heat Transfer 117 (1995) 394–401.

[12] C.L. Yu, R.B. Mesler, A study on nucleate boiling near the peak heat flux through measurement of transient surface temperature, Int. J. Heat Mass Trans. 11 (1993) 827.

[13] P. Sadasivan, C. Unal, R. Nelson, Perspective: issues in CHF modeling – the need for new experiments, Trans. ASME J. Heat Transfer 117 (1995) 558–567.

[14] H. Sakashita, H. Yasuda, H. Kumada, Studies on pool boiling heat transfer: macrolayer thickness in transition boiling, Trans. JSME B 62 (1996) 2322–2330 (in Japanese).

[15] J. Straub, M. Zell, B. Vogel, Pool boiling in a reduced gravity field, in: Proc. 9th Int. Heat Transfer Conf., vol. 1, 1990, pp. 91–112.

[16] T. Oka, Y. Abe, Y.H. Mori, A. Nagashima, Pool boiling of *n*-pentane, CFC, and water under reduced gravity: parabolic flight experiments with a transparent heater, Trans. ASME J. Heat Transfer 117 (1995) 408–417.

[17] M.G. Cooper, A.J.P. Lloyd, The microlayer in nucleate pool boiling, Int. J. Heat Mass Trans. 12 (1969) 895–913.

[18] M.G. Cooper, A.M. Judd, R.A. Pike, Shape and departure of single bubbles growing at a wall, in: Proc. 6th Int. Heat Transfer Conf., vol. 1, 1978, pp. 115–120.

[19] Y.H. Zhao, T. Masuoka, T. Tsuruta, Boiling bubble behavior and heat transfer characteristic on a horizontal Pt-wire within a narrow space, in: Proc. Heat Transfer Seminar of JSME in Okinawa, Japan, 1994, pp. 238–241.

[20] S. Nishio, T. Gotoh, N. Nagai, Observation of boiling structure, in: An Int. Eng. Foundation Conf.: convective flow and pool boiling, Kloster Irsee, Germany, 1997, p. X-4.

[21] R. Hohl, H. Auracher, J. Blum, W. Marquardt, Identification of liquid–vapor fluctuations between nucleate and film boiling in natural convection, 1997, p. II-5.

[22] Y. Haramura, Heat fluctuation while transition and film boiling, in: Proc. 31th National Heat Transfer Symposium of Japan, 1994, pp. 418–420 (in Japanese).

[23] M. Shoji, S. Yokoya, H. Kuroki, in: Proc. 26th National Heat Transfer Symposium of Japan, 3, 1989, pp. 418–420 (in Japanese).

[24] R.F. Gaertner, J.W. Westwater, Population of active sites in nucleate heat transfer, Chem. Eng. Symp. Ser. 56 (1960) 39.

[25] M. Shoji, in: V.K. Dhir, A.E. Bergles (Eds.), Pool and External Flow Boiling, ASME, New York, 1992, p. 237.